Superradiant self-diffraction

A. I. Lvovsky* and S. R. Hartmann
Department of Physics, Columbia University, New York, New York 10027
(Received 9 November 1998)

We calculate the far-field intensity pattern of superradiant emission from an optically thin ensemble of atomic oscillators excited by a spatially nonuniform laser pulse of large Rabi area. As the excitation intensity is increased, the superradiant field develops ring structure and expands due to self-diffraction. This effect is made manifest by a two-pulse photon echo experiment where the second pulse is spatially much broader than the first and has a small Rabi area. As a function of the intensity of the first excitation pulse, we measure the on-axis and off-axis echo intensity and find, in agreement with our calculations, that the two behave differently. We also show that for a random, sufficiently smooth excitation profile, the total power of cooperative emission is proportional to the integral, over the excited volume, of the induced dipole moment squared.
[S1050-2947(99)09305-1]

PACS number(s): 42.50.Fx, 42.25.Fx, 42.50.Md

I. INTRODUCTION

Subsequent to the prediction of superradiance [1], a variety of cooperative phenomena has been studied theoretically and experimentally [2–5]. The theoretical treatment of superradiance involves solving either the optical-Bloch or Maxwell-Bloch equations according to whether the irradiated sample is optically thin or thick. Self-induced transparency [2] experiments are associated with the latter regime and are characterized by propagation effects which reshape the excitation pulse so that it propagates with little loss. On transversing the sample, it moves with reduced velocity and modified length to emerge without any dramatic transformation of its spatial character. For optically thin samples, no reshaping takes place but instead the emerging pulse is followed by an afterwave which is commonly referred to as the free radiation decay [3]. As the optical thickness increases, this afterwave merges with the excitation pulse and the self-induced transparency regime is obtained.

Theoretical treatment of cooperative phenomena normally uses the plane-wave approximation for the generated superradiant field (see, for example, [6]). It is assumed that the geometrical structure of this field reproduces that of the excitation laser beam. This assumption, however, is correct only for the sample geometries of large ($\geqslant 1$) Fresnel numbers and excitation pulses with small Rabi areas. Highly energetic excitation pulses bring about spatial anomalies in the emitted fields. As calculated in [7], an energetic Gaussian excitation pulse being reflected from a saturable absorber interface exhibits ring structure. Another example of spatial structure being modified as the beam propagates through resonantly absorbing plasma of the positive column of the glow discharge in neon is presented in [8].

Both of these papers dealt with optically thick media, which resulted in a necessity to solve a complete system of Maxwell-Bloch equations which could be done only numerically. In the present paper, we study abnormal spatial properties of superradiant emission, which is generated by an optically thin sample when the incident excitation pulse has a large Rabi area and a nonuniform spatial profile. The simplicity of analyzing the optically thin regime brings out the origin of these effects clearly. If the excitation pulse is axially symmetric, so is the induced dipole moment which launches the afterwave. But whereas the amplitude of the excitation pulse decreases monitonically away from the excitation beam axis, the magnitude of the induced dipole moment oscillates as the sine of the Rabi area of the excitation beam at the corresponding off-axis position. Thus the width of the excited region expands with increasing intensity of the excitation pulse (although the latter has constant diameter). In addition, the induced dipole moment has a ring structure. The cooperative electromagnetic field emitted by this complex macroscopic dipole undergoes self-diffraction on its annular pattern, developing is own complicated spatial characteristic. As the excitation pulse is made more intense, the dipole ring pattern compresses, the excited region expands, and the far-field spatial pattern expands.

The experimental observation of the expanded diffraction and ring pattern of a free decay is hampered by the presence of the excitation pulse which immediately precedes it. This pulse is much more intense than the free decay signal and it is not practical for us to shield the detector from it. The solution is to follow the excitation pulse with a second, effectively plane wave, pulse and then look at the far-field spatial pattern of the photon echo that is produced. With the second excitation pulse spatially much broader than the first, the far-field pattern of the echo will reproduce that of the first pulse acting alone, i.e., the free decay. Our experimental arrangement was too noisy to observe the ring pattern but sufficient to measure the spatial expansion of the far-field superrdaiance. But this result by itself is interesting as it arises from an ensemble of radiating dipoles whose spatial extent is increasing with excitation intensity and thus one might mistakenly expect that the observed diffraction pattern would narrow rather than increase.

In the theoretical part of this paper we analyze the geometrical structure of a free polarization decay pulse induced

*Present address: Physics Department, University of California, Berkeley, CA 94720. Electronic address: lvov@socrates.berkeley.edu

by a Gaussian excitation beam and discuss some general properties of the superradiant self-diffracted field. It is followed by a description of a two-pulse photon-echo experiment where the discussed effect of self-diffraction is made manifest.

II. SELF-DIFFRACTION OF A GAUSSIAN BEAM

Consider a coherent optical pulse, directed along $\hat{k}$, incident on an optically thin sample containing a gas of two-level oscillators. Let the spatial profile of the pulse be Gaussian with an intensity I:

$$I = I_0 e^{-2r_\perp^2/r_0^2}, \tag{2.1}$$

where $r_\perp$ is measured from the beam's symmetry axis.

Assume all atoms in the sample were initially in the ground state $|\psi\rangle = |1\rangle$. The pulse then transfers the atoms into a coherent superposition of the ground and excited states:

$$|\psi\rangle = |1\rangle \cos\frac{a(\vec{r})}{2} + i|2\rangle e^{i\vec{k}\cdot\vec{r}} \sin\frac{a(\vec{r})}{2}, \tag{2.2}$$

where the nonuniform Rabi area of the excitation pulse is given by

$$a(\vec{r}) = a_0 e^{-r_\perp^2/r_0^2} \tag{2.3}$$

with

$$a_0 = \sqrt{\frac{8\pi}{c} I_0}\, \frac{d_{12}}{\hbar}\tau, \tag{2.4}$$

where $d_{12} = \langle 1|\hat{D}|2\rangle$ is the dipole moment matrix element and τ is the duration of the excitation pulse. An ensemble of oscillators, each in such a coherent supposition, gives rise to a macroscopic dipole moment, which launches a superradiant afterwave. The magnitude of this dipole moment density is

$$D(\vec{r}) = \langle\psi|\hat{D}|\psi\rangle = N d_{12} \cos\frac{a(\vec{r})}{2}\sin\frac{a(\vec{r})}{2} = \frac{N d_{12}}{2}\sin a(\vec{r}), \tag{2.5}$$

where N is the dipole number density. If $a_0 \ll 1$, $\sin a(\vec{r}) = a(\vec{r})$ and the distribution of the macroscopic dipole moment over the sample area replicates the distribution of the excitation field [Fig. 1(a)]. This is not the case, however, for larger a_0. Figure 1(b) shows the distribution of the dipole moment for the excitation pulse of the same r_0 as in Fig. 1(a) but $a_0 = 4\pi$. The distribution now has a ring structure, with fully excited (deexcited) regions at Rabi areas of odd (even) multiples of π and an induced dipole moment density which is maximum in between. Note that the sign of this dipole moment density oscillates with period 2π.

We proceed by calculating, in the far-field approximation, the superradiant afterwave field, produced by a sample excited in such a manner. This field, measured at $\vec{R}$, is given by

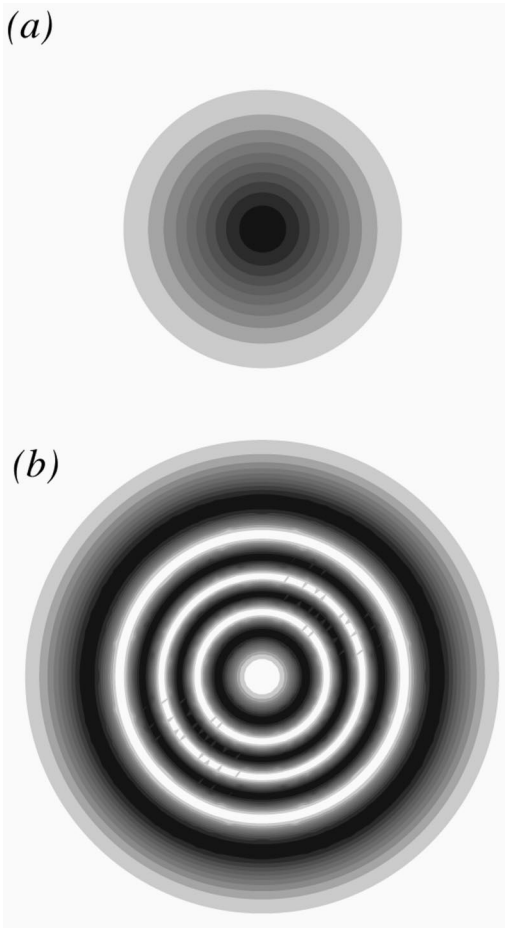

FIG. 1. Distribution of the macroscopic dipole moment $D(\vec{r}_\perp)$ (squared) over the sample cross section. (a) Low excitation pulse area, $a_0 \ll \pi$. The rings visible are due to finite resolution of the computer; actual distribution is smooth. (b) High pulse area $a_0 = 4\pi$; dipole moment distribution exhibits annular character.

$$E_{\vec{R}} = \frac{k^2}{|\vec{R}-\vec{r}|}\int_{\substack{\text{excited}\\\text{volume}}} D(\vec{r}) e^{i\vec{k}\cdot\vec{r} - ik|\vec{R}-\vec{r}|} d\vec{r}. \tag{2.6}$$

For large R, the above expression becomes

$$E_{\vec{R}} = \frac{k^2}{R} e^{-ikR}\int_{\substack{\text{excited}\\\text{volume}}} D(\vec{r}) e^{i\vec{k}\cdot\vec{r} - ik\hat{n}\cdot\vec{r}} dV, \tag{2.7}$$

where $\hat{n} = \vec{R}/R$.

Decomposing $\hat{n} = \vec{n}_{||} + \vec{n}_\perp$ and $\vec{r} = \vec{r}_{||} + \vec{r}_\perp$ into components parallel and perpendicular to $\vec{k}$, we transform the above expression into

$$E_{\vec{R}} = \frac{k^2}{R} e^{-ikR}\int_{\substack{\text{excited}\\\text{volume}}} D(\vec{r}_\perp) e^{ikr_{||}(1-\cos\theta)} e^{-ik\vec{n}_\perp\cdot\vec{r}_\perp} dV, \tag{2.8}$$

where we have set $\vec{n}_{||}\cdot\vec{r}_{||} = r_{||}\cos\theta$, with $\theta = \angle(\vec{k},\vec{n})$. Integrating with respect to $r_{||}$ over the length L of the sample, we obtain

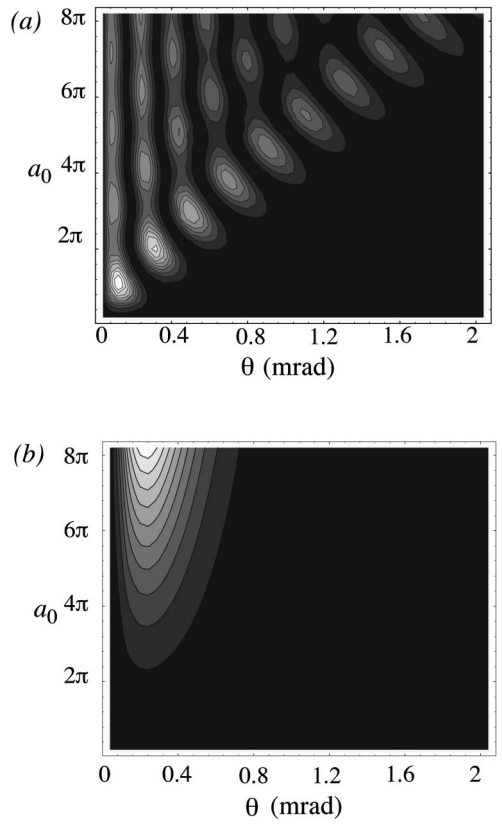

FIG. 2. Electromagnetic energy emitted into the infinitesimal annular solid angle region between θ and $\theta+d\theta$ as a function of a_0 and θ, for the free polarization decay pulse (a) and the excitation pulse (b). For high a_0, the far-field distribution of the free decay beam is characterized by the ring structure and high beam divergence.

$$E_{\vec{R}}=\frac{k^2}{R}\frac{e^{ik(1-\cos\theta)L}-1}{ik(1-\cos\theta)}e^{-ikR}\int D(\vec{r}_\perp)e^{-ik\vec{n}\cdot\vec{r}_\perp}d^2\vec{r}_\perp$$

$$\cong\frac{k^2L}{R}e^{-ikR}\int D(\vec{r}_\perp)e^{-ik\vec{n}\cdot\vec{r}_\perp}d^2\vec{r}_\perp, \tag{2.9}$$

as long as

$$kL(1-\cos\theta)\ll 1. \tag{2.10}$$

For the Gaussian excitation profile (2.3), the above expression transforms into

$$E_{\vec{R}}=2\pi Lr_0^2\frac{k^2}{R}\frac{Nd_{12}}{2}e^{-ikR}$$

$$\times\sum_{n=0}^{\infty}\frac{(-1)^n(a_0)^{2n+1}}{2(2n+1)(2n+1)!}\exp\left(-\frac{(kr_0\theta)^2}{4(2n+1)}\right), \tag{2.11}$$

from which we can calculate the radiated energy along θ.

Figure 2(a) shows the distribution of the superradiant energy in the free decay at θ as a function of a_0 over the range $0<a_0<8\pi$ specialized for the case $\lambda=894$ nm, $r_0=0.5$ mm. At large values of a_0, it has a ring structure and, because of diffraction, is much wider than the excitation beam [see Fig. 2(b)]. All the rings are comparable in size and the number of the rings is approximately equal to the number, a_0/π, of annular regions formed in the sample.

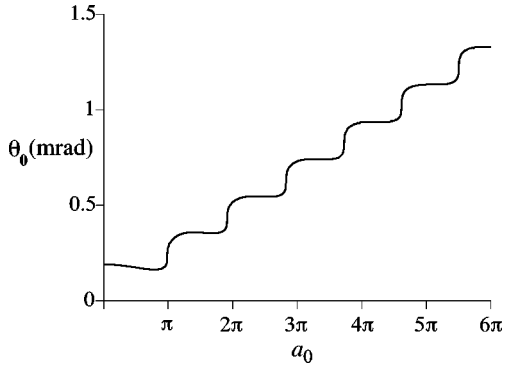

FIG. 3. Angular radius of the entire far-field superradiant beam pattern versus excitation pulse area a_0.

In Fig. 3 we plot the angular radius θ_0 which contains $1-e^{-2}=86.5\%$ of the superradiant beam energy. At low excitation intensity, $a_0\ll\pi$, the induced dipole moment follows the excitation beam profile [Fig. 1(a)]; thus both the free decay and excitation beam have the same angular spread, $(1/\pi)\lambda/r_0=0.19$ mrad, and θ_0 is independent of a_0. As a_0 grows to $\pi/2$, the on-axis induced dipole moment begins to saturate, the effective width of the dipole moment density broadens, and the radiated pattern narrows because of diffraction. For this reason there is the slight decrease in θ_0 with a_0. This behavior continues as the on-axis dipole moment density is further reduced and the radiating volume takes on the shape of a hollow cylinder. At $a_0\cong\pi$, the dipole moment denstiy builds up in a narrow ring-shaped region which leads to a sharp increase in diffraction. As a_0 continues to increase, the size of the excited region expands and a series of more compact annular regions develop (each time a_0 increases by approximately another increment of π) with dipole moment densities in adjacent annular rings alternating in sign. If it were not for the alternation in sign, the far-field free decay pattern would, in fact, narrow with increasing a_0 because of diffraction from the otherwise enlarged radiating sample. But the opposite happens, the far-field pattern broadens, and this can be traced to the combined narrowing of the annular regions and the alternation in sign.

The increased spread in the superradiant emission, relative to the excitation beam, with increasing a_0 gives rise to the possibility for a new method of observing the free polarization decay [3]. The method would be to block the excitation pulse with a circular diaphragm sufficiently small so that the outer rings of the superradiant far-field pattern could still be observed.

Equation (2.9) neglects the interference effects caused by nonzero length (thickness) of the sample. For this approximation to be valid, the angular divergence of the self-diffracted field must be much smaller than $\sqrt{2/kL}$ [here we have used inequality (2.10) and approximated $1-\cos\theta\approx\theta^2/2$]. The angular divergence of the field diffracting off a pattern is on the order of $\lambda/2d$, where d is the characteristic width of the pattern elements. Substituting $\sqrt{2/kL}\gg\lambda/2d$, we find that the validity of the above treatment requires that the

characteristic Fresnel number F' of each individual annular region in the excited sample substantially exceeds one:

$$F' \equiv \frac{4\pi d^2}{\lambda L} \gg 1. \tag{2.12}$$

The width d of these annular regions is inversely proportional to the gradient of $a(\vec{r})$. The above condition can then be rewritten in the form

$$|\nabla a(\vec{r}_\perp)| \ll \sqrt{\frac{4\pi}{\lambda L}} \tag{2.13}$$

everywhere in the sample. For a Gaussian beam with $\lambda = 894$ nm, $r_0 = 1.5$ mm, $L = 1$ cm, this inequality corresponds to $a_0 \ll 18\pi$.

III. FLUORESCENCE AND SUPERRADIANCE

Now we shall obtain the expression for the total power of cooperative free decay emission generated by an optically thin sample excited by an optical pulse of arbitrary spatial profile. As above, we assume that the criterion (2.13) holds. According to Eqs. (2.5) and (2.9), the superradiant field intensity far away from the sample is

$$I_{\vec{R}} = \frac{c}{8\pi}|E_{\vec{R}}|^2 = \frac{ck^4N^2d_{12}^2L^2}{32\pi R^2}\left|\int \sin a(\vec{r}) e^{ik\vec{n}_\perp \cdot \vec{r}} d^2\vec{r}_\perp\right|^2. \tag{3.1}$$

The total power of electromagnetic radiation is obtained by integrating of the above intensity over the solid angle of 4π:

$$\begin{aligned} P_{\rm sr} &= R^2 \int_{\substack{\rm all\\ \rm directions}} I_{\vec{R}} d\vec{n} \\ &= \frac{ck^4N^2d_{12}^2L^2}{32\pi}\int_{\substack{\rm all\\ \rm directions}} \int\int \sin a(\vec{r}_{\perp 1}) \\ &\quad \times \sin a(\vec{r}_{\perp 2}) e^{ik\vec{n}\cdot(\vec{r}_{\perp 2}-\vec{r}_{\perp 1})} d^2\vec{r}_{\perp 1} d^2\vec{r}_{\perp 2} d\Omega, \end{aligned} \tag{3.2}$$

where $d\Omega$ is the differential of the solid angle. To simplify the above, we note that

$$\int_{\substack{\rm all\\ \rm directions}} e^{ik\vec{n}\cdot(\vec{r}_{\perp 2}-\vec{r}_{\perp 1})} d\Omega = 4\pi \frac{\sin k|\vec{r}_{\perp 2}-\vec{r}_{\perp 1}|}{k|\vec{r}_{\perp 2}-\vec{r}_{\perp 1}|} \tag{3.3}$$

and

$$\lim_{k\to\infty} k\frac{\sin k|\vec{r}|}{|\vec{r}|} = 2\pi\delta^2(\vec{r}), \tag{3.4}$$

where $\delta^2(\vec{r})$ is the two-dimensional Diraq delta function. It then follows that, for sufficiently smooth $a(\vec{r})$ [such that $|\nabla a(\vec{r}_\perp)| \ll k$], Eq. (3.2) becomes

$$P_{\rm sr} = \frac{\pi}{4} ck^2N^2d_{12}^2L^2 \int \sin^2 a(\vec{r}_\perp) d^2\vec{r}_\perp. \tag{3.5}$$

We have thus proved the following theorem: for all excitation patterns satisfying inequality (2.13), *the total power of superradiant emission is proportional to the integral, over the excited volume, of the macroscopic dipole moment squared*.

The result (3.5) was obtained in [4] for the case of uniform excitation:

$$a(\vec{r}_\perp) = a_0, \quad r_\perp < r_0 \tag{3.6}$$

and is a manifestation of the fact that the intensity of cooperative emission is proportional to the square of the macroscopic dipole moment density [1]. For such a uniform profile, the intensity $I_{\vec{R}}$ of the field emitted by the sample in each particular direction is proportional to $\sin^2 a_0$, and so is $P_{\rm sr}$ (which is the integral of $I_{\vec{R}}$ over all directions). For a random variable profile $a(\vec{r}_\perp)$, the above result is no longer self-evident, as the field generated in each direction is obtained from interference of fields from various areas of the sample which differ in magnitude and phase. The intensity $I_{\vec{R}}$ along a particular direction is not proportional to $\int |\sin a(\vec{r})|^2 d^2\vec{r}_\perp$. The integral $P_{\rm sr}$ of this intensity over all directions, however, does turn out to be proportional to the above expression.

The above result can be understood using the following qualitative argument. Let us divide the excited volume into a set of cylindrical regions of roughly uniform excitation [so that $a(\vec{r}_\perp) \approx$ const inside each region]. If the Fresnel number of each such region substantially exceeds 1 [i.e., criterion (2.13) holds], the electromagnetic field emitted by this region travels only through its front end and does not enter adjacent regions through their side surface. These elementary regions are not affected by each other's fields and are therefore independent. The total power of the field generated by such a set of independent oscillators is the sum of powers generated by each individual elementary region.

It is also instructive to compare the expression (3.5) with the power of fluorescent (noncooperative) emission from the same sample. The latter is proportional to the total number of atoms in the excited state and is given by

$$P_{\rm fl} = \frac{4}{3} ck^4d_{12}^2N \int_{\substack{\rm excited\\ \rm volume}} \sin^2\left(\frac{a(\vec{r})}{2}\right) d^3\vec{r}. \tag{3.7}$$

Consider a setup in which $P_{\rm sr}$ and $P_{\rm fl}$ are measured while the sample is excited by pulses of constant geometrical profile but variable intensity:

$$a(\vec{r}) = a_0 \alpha(\vec{r}_\perp), \tag{3.8}$$

where a_0 varies from pulse to pulse and $\alpha(\vec{r}_\perp)$ is a constant dimensionless function. Combining Eqs. (3.5) and (3.7), we obtain

$$P_{\rm sr}\left(\frac{a_0}{2}\right) = \frac{3\pi}{16}\frac{NL}{k^2} P_{fl}(a_0). \tag{3.9}$$

The power of the fluorescent and superradiant emissions is described by the same function of the excitation pulse area.

The above equality has been well known [4] for uniform, cylindrical excitation geometries. We have just shown that this connection between coherent and incoherent emissions remains the same for any profile satisfying Eq. (2.13). An

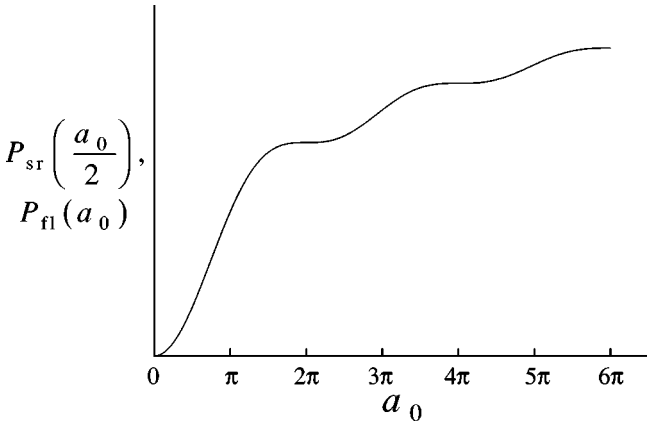

FIG. 4. Total powers of fluorescent and superradiant emission from a sample excited by a Gaussian profile pulse.

example is shown in Fig. 4, where $P_{sr}(a_0/2) \propto P_{fl}(a_0)$ is displayed for Gaussian excitation geometry (2.3).

This function monotonically increases with a_0. Although the geometrical area of the excitation beam remains the same, its increasing Rabi area at the periphery effectively broadens the excited volume (Fig. 1), causing a larger number of atoms to radiate.

IV. EXPERIMENTAL EVIDENCE OF SELF-DIFFRACTION

To demonstrate the existence of self-diffraction, we have performed an experiment on the 894-nm $6S_{1/2}$-$6P_{1/2}$ transition in cesium vapor. We observed the self-diffraction of a photon-echo pulse obtained via two excitation pulses of different geometrical width. The relatively narrow first pulse of high intensity was responsible for inducing the self-diffracting ring pattern in the sample. On the other hand, the second excitation pulse was approximately three times as wide so that it could be considered practically uniform throughout the region of this ring pattern and hence not change it. The advantage of this configuration with respect to observing the self-diffraction of a free polarization decay beam was that the photon echo emerged at an angle and was delayed with respect to the excitation, facilitating the exploration of its spatial structure.

Our laser system was exactly the same, and the optical circuit was almost the same, as that described in [9] (Fig. 5). The 10-ps pulses from a synchronously pumped mode-locked Spectra Physics 375B dye laser were spectrally filtered, amplified, and spatially filtered, resulting in a collimated linearly polarized axially symmetric beam about 3 mm in diameter. About 20% of the beam energy were deflected into an EG&G FND-100 photodetector. The remaining 80% were split into two parts of equal intensity. The second part was spatially expanded via a telescope and then passed through a 25-ns delay line. The two parts were then directed at a 5 mrad angle into a 1 cm quartz sample cell containing saturated cesium vapor at 40 °C.

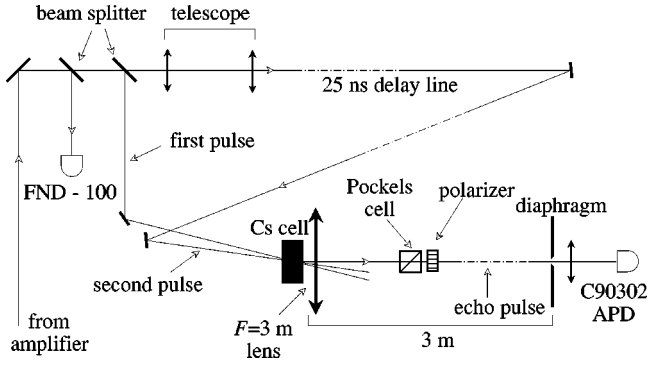

FIG. 5. Experimental setup.

The photon-echo signal generated by the sample pulse was focused by an $F=3$ m lens located immediately after the sample. A 0.7-mm round aperture was mounted on a two-dimensional translation stage in the focal plane of the lens, facilitating the observation of different fragments of the self-diffraction pattern. The aperture was followed by a 1-GHz C90302 EG&G avalanche photodiode, whose output was directed into a 1-GHz 7104 Tektronix oscilloscope. The photon-echo waveforms appearing on the oscilloscope screen were captured by a Tektronix digital camera and stored in an IBM PC compatible computer for future analysis. The excitation pulse intensity registered by the FND-100 diode was integrated by a Stanford Research Systems gated integrator, and then digitized and stored in a Macintosh computer. Since the excitation or laser pump intensity fluctuated considerably, the dependence of the echo intensity over a wide range of pump pulse energies could be obtained by collecting data at a single setting of the laser system.

The leakage of the excitation pulses into the avalanche detector was suppressed via a Pockels cell located behind the sample.

The purpose of this experiment was to present the conceptual evidence of self-diffraction rather than to show complete quantitative agreement of its properties with those outlined in the theoretical part of the paper. The following factors made the latter goal difficult to achieve. First, even despite spectral filtering, the laser spectrum was unstable, resulting in some intensity-independent variation of the excitation pulse area. Second, the excitation pulses were not of perfectly Gaussian profile. Third, the above calculations were made for the free decay self-diffraction rather than photon echo and proper adjustments had to be made to correct for a different experimental method. Fourth, the excitation pulses were just strong enough to create one or two diffrac-

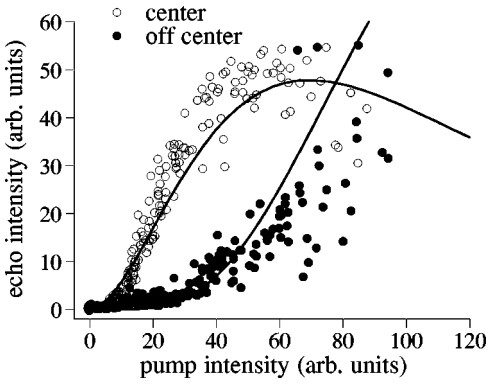

FIG. 6. The photon echo intensity behavior for two different fragments of the self-diffracted far-field pattern are shown along with the theoretical fits. The vertical scale of the off-center data (both theoretical and experimental) is magnified by a factor of 20.

tion rings. Although the Rabi area of the first excitation pulse could be increased in exchange for smaller geometrical area, this would result in a photon-echo signal too weak to observe.

However, major qualitative properties of the self-diffraction effect stay valid in our configuration and can be used to prove its existence. An example is that the higher-order self-diffraction rings appear only when a_0 reaches a certain threshold (see Fig. 2).

The existence of such a threshold for the diaphragm positioned 1.25 mm (0.4 mrad) off the beam center is obvious from Fig. 6. For comparison, the figure also shows the behavior of the photon-echo intensity when the aperture is located at the beam center and no threshold is observed. The graph also shows theoretical fits to both data sets. The theoretical calculations were performed for the photon echo induced by the excitation beams of Gaussian profile with the first beam being three times narrower than the second one. The fit for the centered aperture data was obtained by varying both the horizontal and vertical scales of the obtained dependence to satisfy the least-squares criterion. The same scales were used for the displaced diaphragm data fit, which also shows good agreement. The intensity of the self-diffracted (off-center) echo signal is, however, consistently weaker than the theoretical one, which can be ascribed to the excitation beams being not perfectly Gaussian.

V. CONCLUSION

A macroscopic dipole moment formed by an ensemble of oscillators optically excited by an intense, spatially nonuniform optical pulse forms a ring pattern with dipole moment densities in adjacent annular regions alternating in sign. The superradiant field generated by this ensemble experiences self-diffraction on this pattern, resulting in high beam divergence and, in turn, annular structure of the far field.

The total power of superradiant emission, obtained by integration of the far-field intensity over the solid angle of 4π, is proportional to the integral of the square of the macroscopic dipole moment formed in the sample.

The total power of superradiant emission is determined by the same function of the excitation pulse Rabi area as the total power of noncoherent (fluorescent) emission determined by a function of twice the excitation pulse area.

The effect of superradiant self-diffraction is experimentally demonstrated in a two-pulse photon-echo setting.

[1] R. H. Dicke, Phys. Rev. **93**, 99 (1954).
[2] S. L. McCall and E. L. Hahn, Phys. Rev. **183**, 457 (1969).
[3] R. G. Brewer and R. L. Shoemaker, Phys. Rev. A **6**, 2001 (1972).
[4] I. D. Abella, N. A. Kurnit, and S. R. Hartmann, Phys. Rev. **141**, 391 (1966).
[5] N. Skribanowitz *et al.*, Phys. Rev. Lett. **30**, 309 (1973).
[6] K. Ikeda, J. Okada, and M. Matsuoka, J. Phys. Soc. Jpn. **48**, 1636 (1980).
[7] S. R. Hartmann and J. T. Manassah, Opt. Lett. **16**, 1349 (1991).
[8] V. S. F. Egorov, E. E. Kozlov, and V. V. Reutova, Laser Phys. **2**, 973 (1992).
[9] A. I. Lvovsky and S. R. Hartmann, Laser Phys. **6**, 535 (1996).